Multimode vibronic spectra of the Holstein molecular crystal model

Liu, Qingmei; Ye, Jun; Zhao, Yang

2010

Liu, Q., Ye, J., & Zhao, Y. (2010). Multimode Vibronic Spectra of the Holstein Molecular Crystal Model, Physical Chemistry Chemical Physics, (12), 6045-6053.

https://hdl.handle.net/10356/90391

https://doi.org/10.1039/B925286J

Multimode vibronic spectra of the Holstein molecular crystal model†

Qingmei Liu, Jun Ye and Yang Zhao*

Received 1st December 2009, Accepted 26th February 2010
First published as an Advance Article on the web 9th April 2010
DOI: 10.1039/b925286j

Vibronic spectra of the Holstein model for molecular crystals are investigated using the dynamical mean field theory with the additional aid of the multi-mode Brownian oscillator model. The effects of temperature, intermolecular transfer integral, damping constant and quadratic coupling on the vibronic spectra are examined, and spectra in the presence of two phonon modes are studied in detail. Results from the dynamical mean field theory are corroborated by those from the multi-mode Brownian oscillator model. Strength and weakness of the two approaches are discussed to point out the corresponding regimes of application for each.

I. Introduction

Understanding vibronic spectra of molecular crystals and conjugated polymers is a prerequisite for optimizing organic optoelectronic devices such as light-emitting diodes, organic photovoltaic devices and polymer lasers. One particular type of material are the poly(fluorene)s (PFO)[1] and their derivatives, known for their exceptional quantum efficiency, charge carrier mobility and electro-optical characteristics for applications in optoelectronic devices such as light-emitting diodes. Analysis of the vibronic spectra of such polymers can help understand the optical properties that are determined by electronic excitations and their couplings to dynamic molecular deformations.[2,3]

In recent years, Winokur *et al.*[1,4] have extensively studied optical properties of PFO. For example, the photoluminescence spectra for β-phase at low temperature (usually ~15–20 K) are shown to have well-resolved irregular phonon sidebands.[1] Rigorous Franck–Condon (FC) analysis of photoluminescence spectra and Frenkel-type exciton band structure calculations are performed to understand the steady state spectroscopic properties of the β-phase PFO (and its other phases). Possible multiple-phonon-mode coupling to the electronic transition was revealed, paving the way for additional theoretical techniques including various many-body theories to shed light on the photo-physics of PFO and similar materials. Efforts have also been made to study the role multimode exciton–phonon coupling plays in the photoluminescence spectra of oligothiophene[5] and quaterthiophene[6] single crystals by solving model Hamiltonians with product states and dressed exciton states, respectively. In addition, canonical transformations and Green's functions have been applied recently to derive analytical expressions for linear vibronic spectra of a Frenkel exciton coupled to two phonon modes.[7,8] Considerable differences were found between one-phonon and two-phonon vibronic spectra by the authors. Their theory, however, is perturbative in nature and only applicable in the limit of weak exciton–phonon coupling.[7]

To circumvent the difficulties encountered in the perturbative treatments, it is useful to introduce the dynamical mean field theory (DMFT) to treat exciton–phonon coupling. This many-body technique maps lattice models to corresponding quantum impurity models subject to self-consistency conditions.[9] Beyond the static mean-field treatment, DMFT keeps the full local dynamics induced by local interactions. A powerful many-body technique to study electron–electron and electron–phonon interactions, the DMFT method is capable of interpolating between band-like and atomic-like behavior of electrons. As reported in ref. 10, the DMFT method was firstly applied to the problem of a single electron coupled to a single phonon mode aiming to unravel the small-polaron structure consequently formed. Their results suggested that the DMFT method is exact in the limits of weak and strong couplings and quite efficient in the intermediate regimes. However, for realistic systems such as π-conjugated polymers, there are many optical and acoustic phonon modes, and optical spectra of these materials are dominated by features closely related to multiple-phonon modes. Although path-integral Monte Carlo and momentum-average approximations have been proposed recently to tackle the issue of multiple phonon modes,[11–13] dynamical properties of the generalized Holstein molecular crystal models with multiple phonon modes have not been sufficiently examined.

In this work we will make use of the DMFT method to explicitly compute optical spectra of molecular crystals with exciton–phonon coupling to multiple phonon modes. In addition, a phenomenological approach by the name of multi-mode Brownian oscillator (MBO) model[14,15] is used for comparison. The MBO method was initially designed for understanding optical coherence loss of chromophores in liquids due to solvent dynamics. This model has since been successfully applied to various other systems as its versatile, sophisticated handling of the thermal environment is seldom matched.[3,16,17] The corroboration of the two methods proves fruitful to shed

School of Materials Science and Engineering, Nanyang Technological University, Singapore 639798, Singapore. E-mail: YZhao@ntu.edu.sg
† Electronic supplementary information (ESI) available: Brownian oscillator model and limiting cases. See DOI: 10.1039/b925286j

light on the understanding of the underlying physics of the optical processes and spectral features of molecular crystals and π-conjugated polymers.

The rest of the paper is organized as follows. In section II the DMFT approach is introduced together with associated numerical techniques. In section III, effects of control parameters, such as temperature, transfer integral, damping constant and quadratic coupling, on the vibronic spectra are discussed, in the presence of one or two phonon modes. Results from the DMFT model are compared to those obtained from MBO. Fitting of an experimental PL spectrum of PFO has been carried out toward the end of this section. Conclusions are drawn in section IV.

II. Model and methodology

The original Holstein molecular crystal model[18] involves only linear, diagonal exciton–phonon coupling to one phonon mode. Here we generalize the Holstein molecular crystal model by including two Einstein phonon modes together with their linear and quadratic couplings to the exciton. These phonon modes may possess different symmetries, and the Hamiltonian can be written as

$$\begin{aligned}
\hat{H} &= \hat{H}_e + \hat{H}_p + \hat{H}_{\mathrm{ep}} \\
\hat{H}_e &= \sum_n E_n a_n^\dagger a_n - J\sum_n a_n^\dagger (a_{n+1} + a_{n-1}) \\
\hat{H}_p &= \omega_\alpha \sum_n b_{1,n}^\dagger b_{1,n} + \omega_\beta \sum_n b_{2,n}^\dagger b_{2,n} \\
\hat{H}_{\mathrm{ep}} &= g_\alpha \sum_n a_n^\dagger a_n (b_{1,n}^\dagger + b_{1,n}) + g_\beta \sum_n a_n^\dagger a_n (b_{2,n}^\dagger + b_{2,n}) \\
&\quad + \Delta\omega_\alpha \sum_n b_{1,n}^\dagger b_{1,n} a_n^\dagger a_n + \Delta\omega_\beta \sum_n b_{2,n}^\dagger b_{2,n} a_n^\dagger a_n
\end{aligned} \tag{1}$$

where $a_n^\dagger$ (a_n) denotes the creation (annihilation) operator of a Frenkel exciton on molecule n, E_n is its on-site energy, and J is transfer integral between the neighboring molecules. ω_α describes the frequency of phonon mode α in the system, and its creation (annihilation) operator is denoted as $b_{1,n}^\dagger$ ($b_{1,n}$). Similarly, the other phonon mode in our model is described by ω_β and $b_{2,n}^\dagger$ ($b_{2,n}$). The linear and quadratic exciton–phonon coupling coefficients for 1st (2nd) phonon mode are g_α (g_β) and $\Delta\omega_\alpha$ ($\Delta\omega_\beta$), respectively. Moreover, to facilitate numerical implementation, the uniform on-site energy E_n is regarded as an energy reference point. The Hamiltonian eqn (1) in its present form captures a uniform, translationally invariant aggregate, which is not suitable to describe a disordered system. For more sophisticated Hamiltonians, such as with multiple values of E_n and off-diagonal exciton–phonon coupling, one may need to use more elaborate dynamical mean field methods,[9] which shall be subjects for future studies.

In a DMFT treatment, the lattice model can be mapped onto an impurity Anderson model involving a localized two-level system, labeled by $a^\dagger(a)$, coupled to two local phonons described by $b_{1,0}^\dagger$ ($b_{1,0}$) and $b_{2,0}^\dagger$ ($b_{2,0}$), and hybridized with a fictitious electron conduction band labeled by $c_k^\dagger$ (c_k),

$$\begin{aligned}
\hat{H}_{\mathrm{imp}} &= \sum_k \varepsilon_k c_k^\dagger c_k + \sum_k V_k (c_k^\dagger a + a^\dagger c_k) \\
&\quad + \omega_\alpha b_{1,0}^\dagger b_{1,0} + \omega_\beta b_{2,0}^\dagger b_{2,0} \\
&\quad + g_\alpha a^\dagger a (b_{1,0}^\dagger + b_{1,0}) + g_\beta a^\dagger a (b_{2,0}^\dagger + b_{2,0}) \\
&\quad + \Delta\omega_\alpha b_{1,0}^\dagger b_{1,0} a^\dagger a + \Delta\omega_\beta b_{2,0}^\dagger b_{2,0} a^\dagger a
\end{aligned} \tag{2}$$

where V_k describes the couplings between the local impurity states and the associated bath, and ε_k represents the dispersion of the electrons in the bath. The thermally averaged, retarded one-exciton Green's function is defined as

$$iG_{k,k'}(t) = \theta(t)\langle \exp(i\hat{H}t) a_k \exp(-i\hat{H}t) a_{k'}^+ \rangle \tag{3}$$

where $\theta(t)$ is the unit step function, and $\langle\ \rangle$ denotes the canonical average over the phonon population at temperature $1/\beta$. The Fourier transformation of the Green's function has the form

$$G_{k,k'}(\omega) = \int_{-\infty}^{\infty} \mathrm{d}t \exp(i\omega t) G_{k,k'}(t) \tag{4}$$

with the imaginary part of ω a positive infinitesimal. In the framework of DMFT, the lattice model with translational invariance is mapped into an impurity object embedded in a self-consistently determined effective bath by neglecting all spatial fluctuations in the self-energy. This mapping is exact when the coordination number Z is infinite. It is quite intuitive that the neighbours of a given site can be treated globally as an external bath when their number becomes large, and the spatial fluctuations of the local field are negligible. However, the accuracy of DMFT for three-dimensional systems has been extensively demonstrated.[9] For lower spatial dimensions, the accuracy of DMFT may be compromised by the fluctuations.

Accordingly, the impurity Green's function G_{imp} is defined as

$$G_{\mathrm{imp}}(\omega) = \frac{1}{\omega - \hat{H}_{\mathrm{imp}}} \tag{5}$$

After the initial set of coupling parameters $\{\varepsilon_k, V_k\}$ is chosen, the impurity Green's function G_{imp} and the self-energy function Σ_{loc} are numerically evaluated. By substituting Σ_{loc} into the Dyson equation, the local Green's function G_{latt} can be obtained,

$$G_{\mathrm{latt}}(\omega) = \frac{1}{N}\sum_k \frac{1}{\omega - \varepsilon_k^0 - \Sigma_{\mathrm{loc}}(\omega)}. \tag{6}$$

Here ε_k^0 denotes the non-interacting exciton energy band. Consequently, one can get an updated hybridization function G_0

$$G_0^{-1}(\omega) = G_{\mathrm{latt}}^{-1}(\omega) + \Sigma_{\mathrm{loc}}(\omega) \tag{7}$$

Then the critical problem is how to solve the impurity Green's function and estimate the local self-energy. The impurity Hamiltonian eqn (2) can be separated into $\hat{H}_0$ and $\hat{H}_I$, where $\hat{H}_0$ corresponds to the hybridization function G_0, and $\hat{H}_I$ denotes the local interaction term. This Hamiltonian is similar

to that for a molecule chemisorbed on a solid surface previously investigated,[19,20] and a similar approach is adopted here to estimate the impurity Green's function at zero temperature. Firstly the self-consistent calculations have been carried out due to the existence of the hybridization between local vibrations and the fictitious electron conduction band, which is absent in Cini's Hamiltonian.[19,20] Secondly, the effects of quadratic exciton–phonon coupling interactions can be included in our approach.

The excitonic Green's function can thus be solved by a self-consistency procedure, and the details are included in Appendix A. During the iteration process, a truncation is necessary to put a limit to the maximum number of phonons (N_α, N_β) participating in the scattering process. While there is no analytical expression available for the truncation number (N_α, N_β) to ensure the convergence of the numerical calculations, N_α, for example, is known to be proportional to $g_\alpha^2/J\omega_\alpha$. For convenience, we use a bethe lattice for the noninteracting excitons. The spectral broadening factor η is set at 0.05 for most calculations in this paper. Once the Green's function is determined, the absorption spectrum can be found from the imaginary part of the exciton Green's function[21,22] at zero momentum

$$A(E) = -\frac{1}{\pi}\mathrm{Im}\left[\frac{1}{E - \varepsilon_{k=0} - \Sigma(E)}\right] \qquad (8)$$

At variance with the DMFT method, the MBO model introduces dissipation effects that are omnipresent in real solids into a harmonic oscillator system by coupling the system oscillators linearly to bath modes with a continuous spectrum. In the MBO model, a few primary nuclear coordinates are coupled linearly to an electronic two-level system, and simultaneously, to a bath of secondary harmonic oscillators. The distinction between the primary oscillators and the bath of secondary ones allows interpolation between coherent and damped nuclear movements. Details of the MBO model are included in the ESI.†

III. Results and discussions

In this section, the absorption spectral functions are first calculated to study the effects of temperature, transfer integral, damping constant and quadratic coupling in the presence of one dispersionless phonon mode. The DMFT method is first used, and results are compared with those of the MBO model. The role of linear exciton–phonon coupling in the presence of two phonon modes is discussed next for the extended Holstein model at zero temperature. For the case of one phonon mode, the parameters are chosen as: $g_\alpha = g_\beta = g$, $\omega_\alpha = \omega_\beta = \omega_0$, $\Delta\omega_\alpha = \Delta\omega_\beta = \Delta\omega$ and $N_\alpha = N_\beta = N$, where ω_0 is the frequency of a typical dispersionless phonon mode in molecular crystal systems. All spectral integrals in this paper have been normalized. In addition, we use ω_0 as the energy unit, and scale energy-related variables, *e.g.*, ω, $\omega_{\alpha,\beta}$, γ and k_BT, by ω_0. For convenience, we also set $k_B = 1$.

A Effect of temperature

The finite-temperature spectral calculation for the case of one phonon mode follows that in ref. 20. The results are shown in Fig. 1(a) and (c), where the rescaled temperature, k_BT/ω_0, changes from 0 to 1. As indicated in the inset of Fig. 1(a), the widths of peaks increase dramatically when the temperature rises from 0 to 0.4. However, the widths do not vary greatly when the temperature increases further. It is also noted that the number of the visible phonon sidebands gradually increases as new peaks appear on the lower energy side, thanks to temperature-induced population of phonon states in the electronic ground state. The MBO results are compared to those from the DMFT calculations as shown in Fig. 1(b). From the inset of Fig. 1(b), the broadening of the selected peaks obeys differing rules. It is clear that the linewidth of the peaks increases almost linearly with temperature, especially

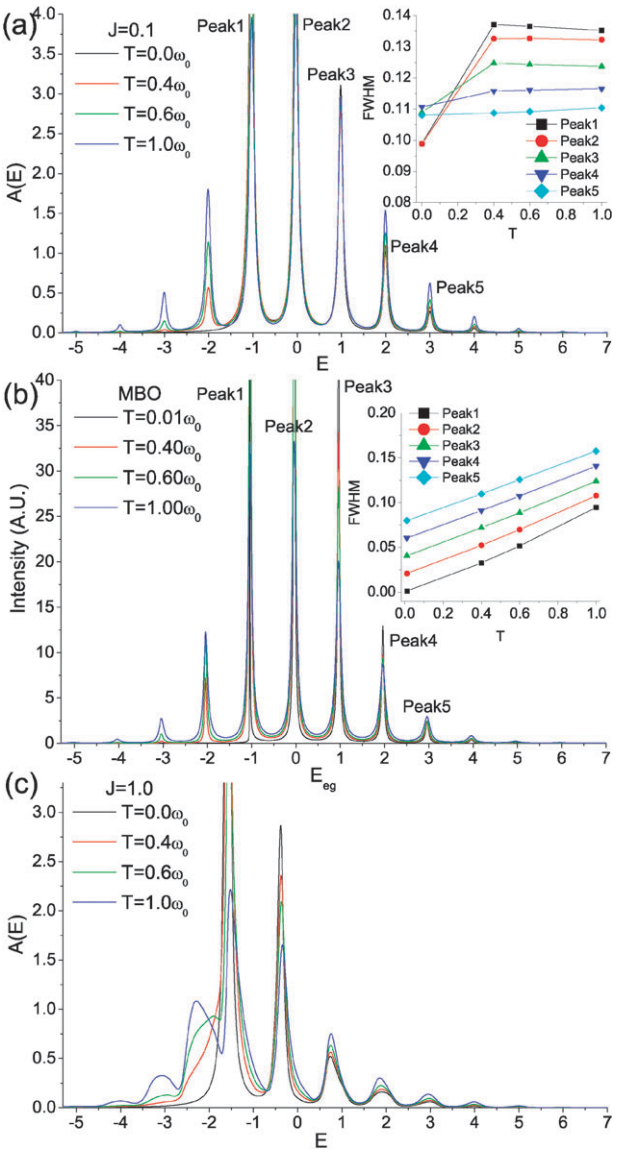

Fig. 1 Absorption spectra calculated from (a) DMFT with $J = 0.1$ and $\Delta\omega = 0.0$; (b) MBO calculated with $\gamma = 0.02$; (c) DMFT with $J = 1.0$ and $\Delta\omega = 0.0$. The inset of (a) shows FWHM *vs.* temperature for the first five peaks of the DMFT spectra. The inset of (b) displays FWHM *vs.* temperature for the first five peaks of the MBO spectra. The other parameters for the calculations are: $S = g^2 = 1.0$ and $\omega = 1.0$. For the DMFT calculations, N is set to 60.

for low temperatures (*e.g.*, $T < 0.6$), in agreement with ref. 23. This effect is mainly due to an increase in occupation of the phonon bath in the MBO model, where more secondary phonons participate in the dissipation processes, resulting in a lifetime reduction of the exciton–phonon entity responsible for the sidebands. From this point of view, the difference between the linewidths of the two models may be mainly due to the sophisticated treatment of the phonon bath in the MBO method. In the DMFT model, only optical phonons participate in the scattering of the exciton, the increase in temperature may only affect the lifetime of the exciton when the temperature is relatively low, as demonstrated in the inset of Fig. 1(a). As shown in Fig. 1(b), new peaks become visible on the lower energy side with increasing temperature as more phonons participate in the exciton–phonon scattering processes.[24] One also observes a strong enhancement of the polaron effective mass accompanied by further bandwidth narrowing[25] with increasing temperature. For the DMFT spectra with a relatively large transfer integral J, as shown in Fig. 1(c), the linewidth of the phonon sidebands have a complicated dependence on temperature, which may be related to the competing effects of a sizable exciton–phonon coupling strength and a relatively large value of the exciton transfer integral.

B Effect of transfer integral *J*

In a molecular stack, exciton hopping substantially affects molecular vibronic spectra. In the MBO model,[23] this term is not taken into account as only two electronic levels are considered. While the assumption of a weak intermolecular transfer is often made for the Frenkel excitons,[8] the transfer integral is non-perturbatively taken into account in our DMFT method so that its effects on the vibronic spectra can be examined in details. The calculated results are displayed in Fig. 2 for the case of $g = 1.0$ and $\Delta\omega = 0.0$. It can be found that with increasing J (from 0.1 to 1.0), the peak positions are red-shifted almost linearly with J (*i.e.*, towards the low frequency region), while the spectral weights are gradually

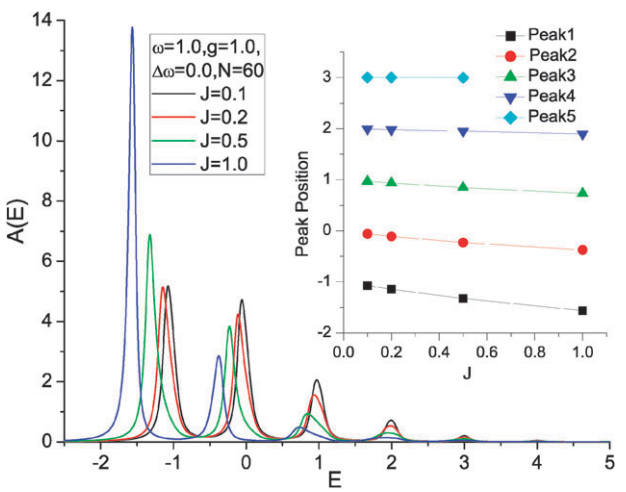

Fig. 2 DMFT absorption spectra for various values of transfer integral J, $T = 0$ and $g = 1.0$. The exciton–phonon coupling is assumed to be linear here. The peak position as a function of J for the first five peaks is shown in the inset.

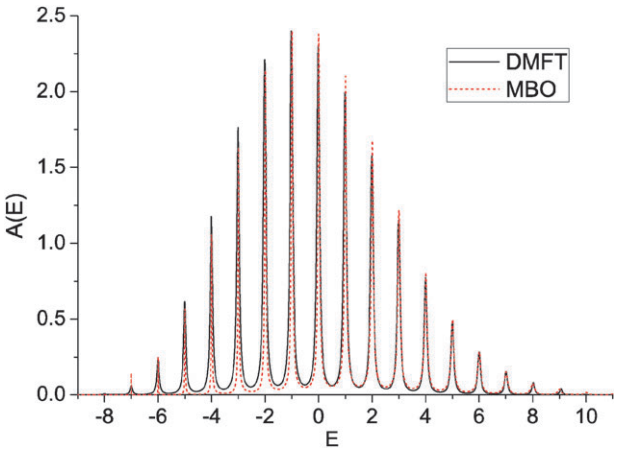

Fig. 3 Comparison of absorption spectra calculated from DMFT and MBO. For the DMFT spectrum, the parameters are: $J = 1$, $g^2 = 8.0$, $\Delta\omega$, $N = 60$, and $T = 0.0$. For the MBO spectrum, the parameters are: $S = g^2 = 8.0$, $T = 0.01$, $\gamma = 0.01$ and $E_{eg} = -7.0$. $\omega = 1.0$ in both spectra.

transferred to lower peaks (*i.e.*, the effective values of exciton–phonon coupling is reduced). Known as the motional narrowing effect, the increase in J leads to the suppression of simultaneous phonon excitations. Such an effect is also clearly observed by comparing the DMFT spectrum ($J = 1$) to the MBO spectrum, as shown in Fig. 3, since the DMFT model actually reduced to the Huang–Rhys theory[26] when T, J and $\Delta\omega$ equal 0 (see the ESI for details†). Thus, the comparison in Fig. 3 is a direct evidence of the effect of J in transferring spectral weight towards lower energy peaks and consequently lowering the effective g.

C Effect of damping factor *η*

The effect of the damping constant η on the vibronic spectra is displayed in Fig. 4(a), while the effect of γ on the MBO spectra is shown in Fig. 4(b) for comparison. The spectral damping constant η has a relatively simple interpretation since it is directly related to the lifetime of the exciton. The relationship between η and width is obvious from the inset of Fig. 4(a) since the linewidths of the peaks are proportional to η. However, for the spectra calculated with the MBO model[23] as shown in the inset of Fig. 4(b), the broadening due to the damping constant γ is more complicated, with added sophistication attributed to the coupling of the primary phonon mode(s) to the bath phonons in the MBO model. Due to the lack of a secondary phonon bath in the DMFT calculation, the lifetime of the exciton is determined phenomenologically by η, resulting in a clear Lorentzian lineshape as shown in Fig. 4(a). However, as indicated from Fig. 4(a) and (b), dephasing due to the presence of an external bath plays an important role in determining the overall spectral lineshape. To achieve a better description of optical spectral features, it is critical that the merits of the two methods be combined. Recently, efforts have been made to use a non-Markovian form of spectral density to describe optical absorption and energy transfer dynamics in a molecular aggregate,[27] again pointing to the importance of a dissipative bath to ultrafast relaxation dynamics.

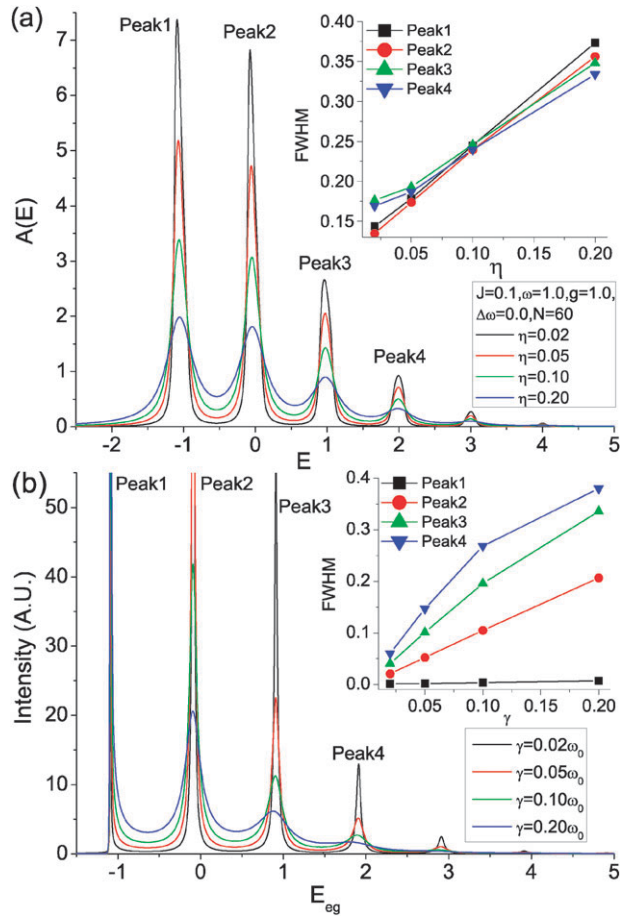

Fig. 4 Absorption spectra calculated from (a) DMFT for $T = 0$, $J = 0.1$ and $\Delta\omega = 0.0$. (b) MBO for $T = 0.01$. The inset of (a) shows FWHM *vs.* η for the first four peaks for the DMFT spectrum. The inset of (b) shows FWHM *vs.* γ for the first four peaks of the MBO spectra. Other parameters for both calculations are: $S = g^2 = 1.0$ and $\omega_0 = 1.0$

D Effect of quadratic exciton–phonon coupling

The quadratic exciton–phonon coupling is considered to be dominant for the non-totally symmetric molecular vibrations, where the phonons are localized to a molecule.[28] As known from eqn (1), the $\Delta\omega$ term actually represents the relative phonon frequency shift in the excited molecule. In order to study the effect of the $\Delta\omega$ term, we first consider the case of $g \ll 1$, $J \ll 1$, where the quadratic coupling must be taken into account since such interaction is energetically more important than the linear coupling term.[21] The parameters adopted for this case are $J = 0.1$ and $g^2 = 0.01$, and the value of $\Delta\omega$ varies from 0.0 to 2.0. The calculated absorption spectra are displayed in Fig. 5, where the bottom spectrum corresponds to the limiting case with $g = 0$, and $\Delta\omega = 0$. With increasing $\Delta\omega$, the spectral features change from the free-exciton type to that with an additional one-phonon sideband form (primarily due to the weak linear exciton–phonon coupling here, only a one-phonon sideband is resolved). The spacing between two peaks are strongly dependent on the value of $\Delta\omega$, which manifests the effect of this term in determining the relative phonon frequency shift in the excited molecule. What is more interesting is the observation of the transfer of spectral weight

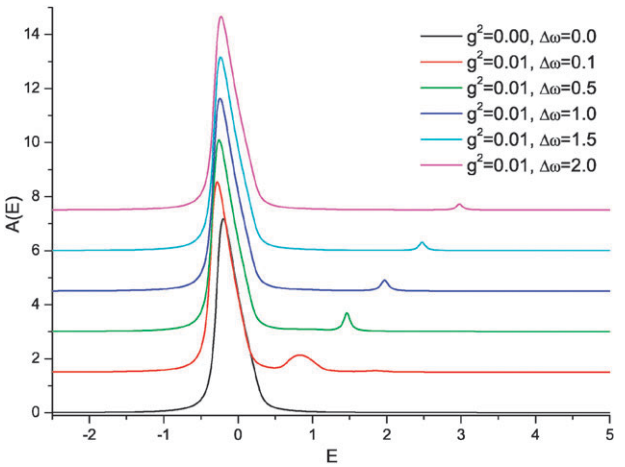

Fig. 5 Absorption spectra in the weak-coupling regime with various quadratic coupling $\Delta\omega$, where $J = 0.1$, $\omega = 1.0$, $N = 60$ and $T = 0$.

of the phonon sideband to the major peak and increase of relative intensity ratio between first and second peak as $\Delta\omega$ increases. This phenomenon is even more pronounced for cases with larger g. As demonstrated in Fig. 6, the quadratic coupling $\Delta\omega$ strongly influences the absorption spectra. It is also noted that the maximum phonon number $N_\alpha(N_\beta)$ must be large enough to guarantee the convergence of the spectral calculation with a large value of J. The peak position is plotted as a function of the peak number in the inset of Fig. 6 for values of $\Delta\omega$ from 0.0 to 3.0.

E The spectra with two phonon modes

We turn to the case with two dispersionless phonon modes. The ground state properties, in the context of polaronic self-trapping

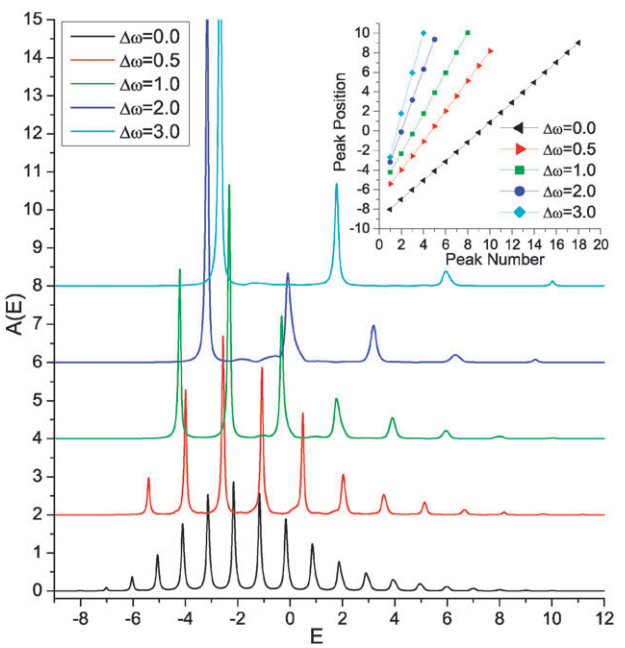

Fig. 6 Absorption spectra in the strong-coupling regime, where $J = 1.0$, $\omega = 1.0$, $g^2 = 8.0$ and $T = 0$. Inset of the figure displays the peak position *vs.* peak number of the spectra for various values of the quadratic coupling $\Delta\omega$.

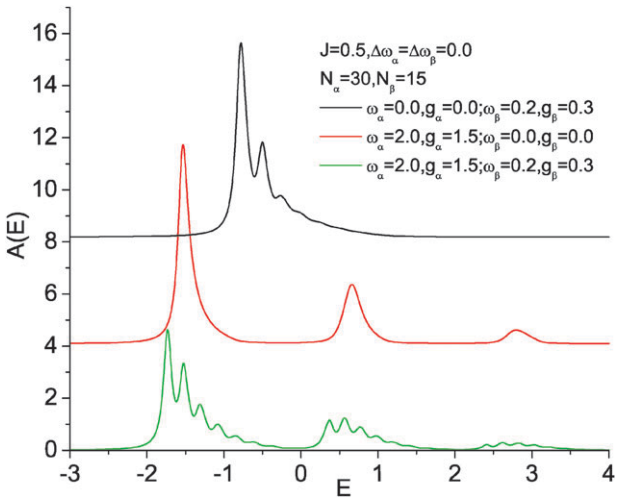

Fig. 7 Comparison of a two mode DMFT spectrum and single mode spectra corresponding to each phonon mode used in the two mode calculation. The parameters chosen for each spectrum are also shown in the figure.

transition, are determined by the mode coupled more strongly to the exciton.[12] In order to study the effects on the properties on the high-energy regime, we consider two cases of varying exciton–phonon couplings. For the weak coupling case, the parameters are $J = 0.5$, $\Delta\omega_\alpha = \Delta\omega_\beta = 0.0$, $N_\alpha = 30$, $N_\beta = 15$. For the first mode, $\omega_\alpha = 2.0$ and $g_\alpha = 1.5$, while for the second mode, $\omega_\beta = 0.2$ and $g_\beta = 0.3$. The absorption spectra are displayed in Fig. 7. The spectrum in the sole presence of the β-mode shows a phonon progression despite the small phonon frequency and weak coupling. When two phonon modes are simultaneously taken into account, the effects of the two types of phonon excitations are combined to yield the overall absorption lineshape at the bottom of Fig. 7. The overall lineshape is found to be composed of both types of phonon excitations despite their large difference in phonon frequency. As the phonon excitations are effectively coupled through the band continuum, even the weak coupling to the second phonon mode will have effects on the lineshape in the high-energy regime of the overall spectrum.

When the couplings to the two phonon modes are comparable in strength, some interesting features may appear in the high-energy portion of the spectra. We first consider the case with $\omega_\alpha = 1.0$, $g_\alpha = 1.0$, $\omega_\beta = 1.5$ and $g_\beta = 1.0$, as shown in Fig. 8(a). Other parameters for the case are $J = 0.2$, $\Delta\omega_\alpha = \Delta\omega_\beta = 0.0$, $N_\alpha = N_\beta = 30$. The spectra with a single phonon mode are also shown as a reference. For the bottom spectrum with two phonon modes, the spacing between the lowest exciton band and the one-phonon continuum corresponds to the value of ω_α, while for higher energy states, the spacings all equal to 0.5, which is the difference of the two frequencies, *i.e.*, $|\omega_\alpha - \omega_\beta| = 0.5$. To gain a better understanding of the DMFT spectra, the MBO counterpart and their peak positions are plotted in Fig. 8(b) and its inset, respectively. It is clear that for the single-mode spectra, the phonon sidebands are equally spaced as shown in the inset of Fig. 8(b), and the peak position *vs.* peak number plots from the two methods are in close agreement. However, due to

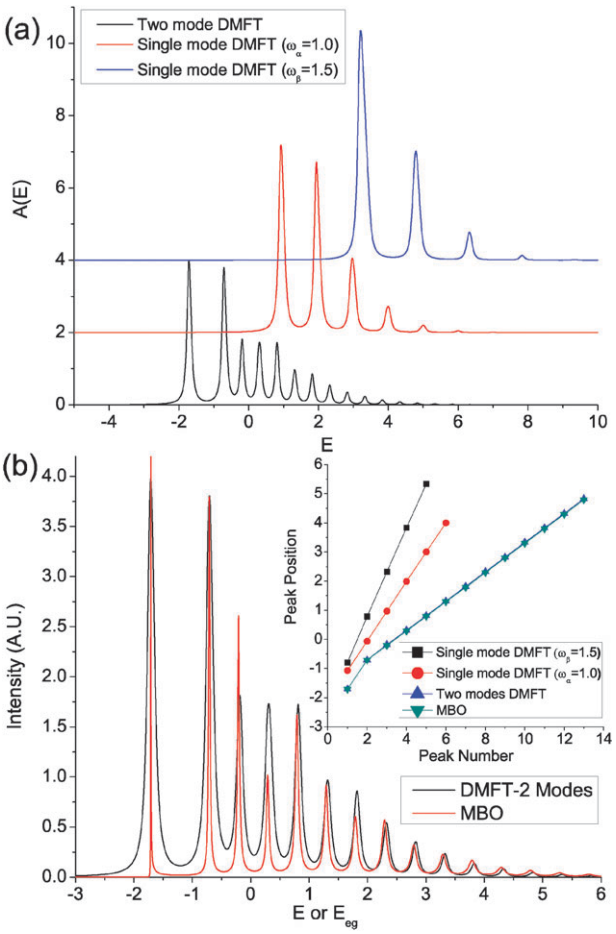

Fig. 8 The DMFT absorption spectrum with $\omega_\alpha = 1.0$, $g_\alpha = 1.0$, $\omega_\beta = 1.5$, $N_\alpha = N_\beta = 30$, and $g_\beta = 1.0$, single mode spectra (mode α and β) are also displayed for comparison. (b) Comparison of DMFT and MBO spectrum, where the MBO paramters are: $S_1 = S_2 = 1.0$, $\omega_1 = 1.0$, $\omega_2 = 1.5$ and $\gamma_1 = \gamma_2 = 0.025$.

the difference of the two models in treating dissipative effects and the two-level nature of the MBO model, the two spectra in Fig. 8(b) differ substantially, reminding us the importance of bath dephasing and exciton transfer integral J to shaping the spectral features.

As mentioned in the Introduction, the DMFT approach is applicable to cases with a wide range of the transfer integral J. Anthracene, for example, is one type of aromatic crystal with strong intermolecular transfer.[7,8,29,30] Vibronic spectra of anthracene reveal two relevant phonon modes with two sets of parameters: $\omega_\alpha = 1400\ \text{cm}^{-1}$, $g_\alpha^2 = 0.9$ and $\omega_\beta = 400\ \text{cm}^{-1}$, $g_\beta^2 = 0.15$. Data on the longitudinal-transversal splitting[29] gives an estimation of the exciton transfer integral J of approximately 300–400 cm^{-1}. In ref. 7, the authors used an analytical expression to calculate the absorption spectra for a one-dimensional anthracene-like aggregate, violating their original assumption of weak exciton transfer. Here we set $\omega_0 = 806\ \text{cm}^{-1}$ as the energy unit, and the relevant parameters are $\omega_\alpha = 1.736\omega_0$, $\omega_\beta = 0.496\omega_0$ and $J = 0.372$–$0.496\omega_0$. Calculated DMFT spectra are displayed in Fig. 9 with the case of $J = 40\ \text{cm}^{-1}$ used as a comparison. For $J = 40\ \text{cm}^{-1}$, the first narrow peak corresponds to one-particle (bound)

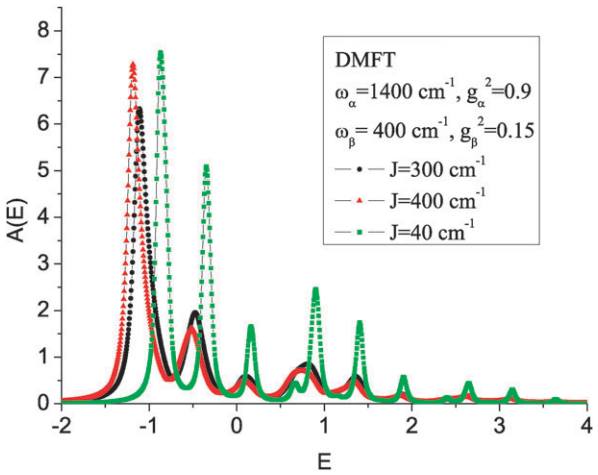

Fig. 9 The DMFT absorption spectrum for the anthracene with $\omega_\alpha = 1400\ cm^{-1}$, $g_\alpha^2 = 0.9$, $\omega_\beta = 400\ cm^{-1}$, $g_\beta^2 = 0.15$, and $J = 300\ cm^{-1}$, $400\ cm^{-1}$ and $40\ cm^{-1}$.

exciton–phonon state. The second and third peaks are located at ω_β and $2\omega_\beta$, respectively, while the fourth peak is at ω_α. These results are consistent with those in ref. 29. When J assumes a realistic value of $300\ cm^{-1}$, the absorption spectrum is red-shifted considerably with almost every peak broadened compared to $J = 40\ cm^{-1}$. The high-energy absorption peaks are from many-particle states in the coupled exciton–phonon system.

The DMFT method described in this paper is also useful to interpret spectra from materials such as poly(fluorene)s (PFO). As shown in Fig. 10, the unit of energy in the DMFT approach is equal to 0.1 eV. The MBO results are also shown to illustrate the effects of the phonon bath and finite temperature.

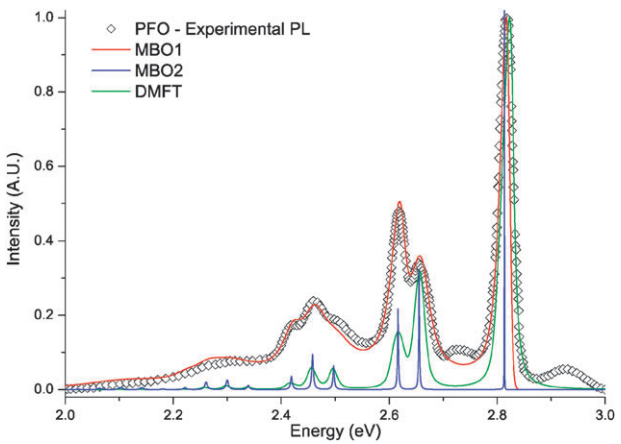

Fig. 10 Comparison of DMFT and MBO fitting of the experimental β-phase poly(fluorene) (PFO) photoluminescence (PL) spectrum[1] measured at 25 K. The DMFT parameters are: $\omega_1 = 1.58$, $\omega_2 = 1.98$, $S_1 = 0.77$, $S_2 = 0.64$, $J = 0.1$ and $\eta = 0.05$. The MBO1 parameters are: $\omega_1 = 1275\ cm^{-1}$, $\omega_2 = 1590\ cm^{-1}$, $\omega_3 = 100\ cm^{-1}$, $S_1 = 0.75$, $S_2 = 0.64$, $S_3 = 0.95$, $\gamma_1 = 240\ cm^{-1}$, $\gamma_2 = 105\ cm^{-1}$, $\gamma_3 = 200\ cm^{-1}$, and $E_{eg} = 2.825$ eV. The MBO2 parameters are the same as those of MBO1 except for $\gamma_1 = 12.75\ cm^{-1}$ and $\gamma_2 = 15.9\ cm^{-1}$. And only the coupling of ω_1 and ω_2 are considered. The DMFT and MBO spectra are both normalized, where the x-axis of the DMFT spectrum has been scaled by 10 in order to fit the PFO spectrum.

The DMFT spectrum agrees with experimental spectrum for the first two peaks, the difference is mainly attributed to the absence of a secondary phonon bath which is included in the MBO model. By reducing the damping factors in the MBO model to a relatively low value, a much better agreement between the two models can be obtained. A spectrum calculated from an underdamped MBO model, labeled as MBO2 in Fig. 9, recovers the DMFT spectrum qualitatively, suggesting the important role of the dissipative phonon bath in determining spectral features in realistic scenarios. By fine tuning the damping behavior of the secondary phonon bath in the MBO model, the spectrum labeled as MBO1 is found to be in good quantitative agreement with the experimental spectrum. There are also some features not fully reproduced by the MBO model, such as the small peak around $700\ cm^{-1}$ away from the ZPL, assigned as the phonon sideband for the $700\ cm^{-1}$ mode in the β-phase PFO according to Winokur *et al.*[1] By incorporating these factors that affect the spectral features in the MBO calculations, it is possible to achieve better quantitative agreement with experiment. Moreover, from the semi-empirical together with rigorous Frank–Condon analysis performed by Winokur *et al.*,[4] the dominant (*e.g.*, with $S > 0.15$) phonon modes in the PL spectrum of β-phase PFO (measured at $T = 18$ K) were determined as: $\omega_1 = 1605\ cm^{-1}$, $\omega_2 = 1282\ cm^{-1}$ and $\omega_3 = 61\ cm^{-1}$; with the Huang–Rhys factors: $S_1 = 0.30$, $S_2 = 0.17$ and $S_3 = 0.75$, respectively. By comparing these with the MBO fitting results shown in Fig. 9, a qualitative agreement is obtained. The S values obtained by MBO are slightly higher due to the presence of the dissipative phonon bath in this model, pointing to the sensitivity of the PL spectra of β-phase PFO to temperature and importance of the dissipative phonon baths.

IV. Conclusions

Despite more than six decades of investigation, the Holstein polaron remains a topic of great interest.[31–33] A variety of approximate methods have been used to study static and dynamic properties of the coupled exciton–phonon system such as a hierarchy of time-dependent variational trial states enlisted recently to spearhead the attack on Holstein polaron dynamics.[34] Also worth mentioning is a powerful method of diagrammatic quantum Monte Carlo put forward with no restriction for the form of particle–phonon interaction and dimensionality of the problem.[32,33] In addition, the dynamical coherent potential approximation in combination with the Hartree approximation (HA-DCPA) was employed by two of the authors to study off-diagonal exciton–phonon coupling,[31] dispersive phonons and multiexcitons. In this work, by applying the DMFT method, we have investigated systematically the vibronic spectra of the extended Holstein model with linear and quadratic exciton–phonon interactions to one or two phonon modes. In the presence of one phonon mode, the effects of temperature, transfer integral, damping constant and quadratic coupling on the vibronic spectra have been studied in detail. For weak linear exciton–phonon coupling, the introduction of quadratic coupling blueshifts the one-phonon side band due to modulation of the effective phonon energy.

For strong linear exciton–phonon coupling, the quadratic term shifts the positions of vibronic peaks while reducing the effective coupling strength. Increasing temperature can result in the formation of new peaks on the lower energy side while introducing thermal broadening to the spectral peaks. In the presence of two phonon modes, even very weak coupling to the second phonon will bring pronounced effects to the vibronic spectra. The two phonon modes are found to be inextricably coupled, and their interactions are facilitated indirectly by the exciton band. When the second phonon mode is comparable in energy to the first one and both modes have similar coupling strength, vibronic spectra will display non-uniform peak spacings in contrast to the equal spacings for one phonon mode. Similar behavior is also found in the spectra calculated by the MBO model.

We have compared spectra calculated from DMFT with those from the MBO model with respect to spectral features such as lineshapes and linewidths. Such comparisons indicate that, when J/S, T and $\Delta\omega$ are negligible compared to ω_0, these methods are in principle equivalent. However, in the presence of relatively large values of J and $\Delta\omega$, the DMFT approach can provide additional features that are not fully described by the MBO model. The DMFT approach fails to account for the effect of temperature on the linewidth properly due to the absence of a sophisticated phonon bath. Attempts has also been made to employ both the DMFT and MBO methods to fit the experimental low-temperature (20 K) PL spectrum of the β-phase PFO. While individually the MBO approach is shown to produce a better quantitative agreement with the experimental results than the DMFT counterpart, in combination the two methods can generate qualitative insights into the PFO spectra. It is shown from the comparison of the results from both methods that secondary dissipative phonon bath has an important role in determining spectral features of realistic materials. Thus, it is meaningful to combine the DMFT approach described in this paper with the MBO model to probe optical processes in organic molecular crystals and conjugated polymers.

Appendix: The self-consistency procedure

Here, we introduce a general continued-fraction algorithm to recursively solve the impurity self-energy and Green's function for the system with two phonon modes. Below we sketch a derivation, which follows the ideas of ref. 19.

First of all, let us introduce two auxiliary quantities as

$$G(m,n,z) = \langle 0,0,0|b_{1,0}^{m} b_{2,0}^{n} (z-\hat{H}_{\mathrm{imp}})^{-1}|0,0,0\rangle$$

$$G_0(m,n,z) = \langle 0,0,0|(z-\hat{H}_0 - m\omega_\alpha - n\omega_\beta)^{-1}|0,0,0\rangle \quad \text{(A1)}$$

By using the operator identities as follows,

$$\frac{1}{z-\hat{H}_{\mathrm{imp}}} = \frac{1}{z-\hat{H}_0} + \frac{1}{z-\hat{H}_0}\hat{H}_1\frac{1}{z-\hat{H}_{\mathrm{imp}}} \quad \text{(A2)}$$

$$b_{1,0}^{m} b_{2,0}^{n} (z-\hat{H}_0)^{-1} = (z-\hat{H}_0 - m\omega_\alpha - n\omega_\beta) b_{1,0}^{m} b_{2,0}^{n}$$

the solution of the impurity Green's function will be reduced to a system of recursive equations in terms of $G(m, n, z)$,

$$\begin{aligned} G(m,n) &= \delta_{m,0}\delta_{n,0}G_0(0,0) \\ &\quad + G_0(m,n)\,[g_\alpha(G(m+1,n) + mG(m-1,n)) \\ &\quad + g_\beta(G(m,n+1) + nG(m,n-1)) \\ &\quad + \Delta\omega_\alpha m G(m,n) + \Delta\omega_\beta n G(m,n)] \end{aligned} \quad \text{(A3)}$$

The set of recursive equations can be further transformed into a generalized continued fraction by defining auxiliary quantities,[19]

$$\begin{aligned} \Lambda(m,n,p,q) &= \delta_{mp}\delta_{nq} \\ &\quad - G_0(m,n)\,[g_\alpha(\delta_{p,m+1} + m\delta_{p,m-1})\delta_{q,n} \\ &\quad + g_\beta(\delta_{q,n+1} + n\delta_{q,n-1})\delta_{p,m} \\ &\quad + \Delta\omega_\alpha m\delta_{p,m}\delta_{q,n} + \Delta\omega_\beta n\delta_{q,n}\delta_{p,m}] \end{aligned} \quad \text{(A4)}$$

then the equations regarding to $G(m, n)$ can be rewritten the following form

$$\sum_{p,q}\Lambda(m,n,p,q)\,G(p,q) = \delta_{m,0}\delta_{n,0}G_0(0,0) \quad \text{(A5)}$$

where the non-zero matrix elements of $\Lambda(m, n, p, q)$ can be written as

$$\begin{aligned} D_{\mathrm{mp}}^{\mathrm{nq}} &= \Lambda(m,n,p,q) = \delta_{m,p} \\ &\quad - g_\alpha G_0(m,q)(\delta_{p,m+1} + m\delta_{p,m-1}) \\ &\quad - \Delta\omega_\alpha m\delta_{pm}G_0(m,q) - \Delta\omega_\beta q\delta_{pm}G_0(m,q) \end{aligned}$$

$$\begin{aligned} E_{\mathrm{mp}}^{\mathrm{nq}} &= \Lambda(m,q-1,p,q) = -g_\beta G_0(m,q-1)\delta_{mp} \\ F_{\mathrm{mp}}^{\mathrm{nq}} &= \Lambda(m,q+1,p,q) = -g_\beta(q+1)G_0(m,q+1)\delta_{mp} \end{aligned} \quad \text{(A6)}$$

As indicated by eqn (A2), $\Lambda(m, n, p, q)$ is a series of three diagonal matrices in the nq indices and its elements are the same type of matrices in the mp indices. Thus the component $G(0,0)$ can be expressed in a matrix of continued fraction as

$$G(0,0) = G_{\mathrm{imp}} = K_{00}G_0(0,0)$$

$$K = \cfrac{1}{D^{00} - E^{01}\cfrac{1}{D^{11} - E^{12}\cfrac{1}{D^{22} - \cdots}F^{21}}F^{10}} \quad \text{(A7)}$$

Acknowledgements

Support from the Singapore Ministry of Education through the Academic Research Fund (Tier 2) under Project No. T207B1214 is gratefully acknowledged.

References

1 M. J. Winokur, J. Slinker and D. L. Huber, *Phys. Rev. B: Condens. Matter Mater. Phys.*, 2003, **67**, 184106.
2 A. S. Davydov, *Theory of Molecular Excitons*, Plenum, New York, 1971.

3 Y. Zhao and R. S. Knox, *J. Phys. Chem. A*, 2000, **104**, 7751; J. Ye, A. Grimsdale and Y. Zhao, *J. Phys. Chem. A*, 2010, **114**, 504; F. Gao, W. Z. Liang and Y. Zhao, *J. Phys. Chem. A*, 2009, **113**, 12847; L. T. Su, A. Tok, Y. Zhao, N. Ng and F. Y. C. Boey, *J. Phys. Chem. B*, 2009, **113**, 5974.
4 W. Chunwaschirasiri, B. Tanto, D. L. Huber and M. J. Winokur, *Phys. Rev. Lett.*, 2005, **94**, 107402.
5 Z. Zhao and F. C. Spano, *J. Phys. Chem. C*, 2007, **111**, 6113–6123.
6 L. Silvestri, S. Tavazzi, P. Spearman, L. Raimondo and F. C. Spano, *J. Chem. Phys.*, 2009, **130**, 234701.
7 I. J. Lalov and I. Zhelyazkov, *Chem. Phys.*, 2008, **352**, 185.
8 I. J. Lalov and I. Zhelyazkov, *Phys. Rev. B: Condens. Matter Mater. Phys.*, 2007, **75**, 245435; I. J. Lalov and I. Zhelyazkov, *Phys. Rev. B: Condens. Matter Mater. Phys.*, 2006, **74**, 035403.
9 A. Georges, G. Kotliar, W. Krauth and M. J. Rozenberg, *Rev. Mod. Phys.*, 1996, **68**, 13; G. Kotliar, S. Y. Savrasov, K. Haule, V. S. Oudovenko, O. Parcollet and C. A. Marianetti, *Rev. Mod. Phys.*, 2006, **78**, 865.
10 S. Ciuchi, F. D. Pasquale and S. Fratini, *Phys. Rev. B: Condens. Matter*, 1997, **56**, 4494.
11 G. L. Goodvin, M. Berciu and G. A. Sawatsky, *Phys. Rev. B: Condens. Matter Mater. Phys.*, 2006, **74**, 245104.
12 L. Covaci and M. Berciu, *Europhys. Lett.*, 2007, **80**, 67001.
13 P. E. Kornilovitch, *Phys. Rev. B: Condens. Matter Mater. Phys.*, 2006, **73**, 094305.
14 S. Mukamel, *Principles of Nonlinear Optical Spectroscopy*, Oxford University Press, Oxford, 1995.
15 R. S. Knox, G. J. Small and S. Mukamel, *Chem. Phys.*, 2002, **281**, 1.
16 S. L. Shi, G. Q. Li, S. J. Xu, Y. Zhao and G. H. Chen, *J. Phys. Chem. B*, 2006, **110**, 10475.
17 S. J. Xu, G. Q. Li, Y. J. Wang, Y. Zhao, G. H. Chen, D. G. Zhao, J. J. Zhu and H. Yang, *Appl. Phys. Lett.*, 2006, **88**, 083123.
18 T. Holstein, *Ann. Phys.*, 1959, **8**, 325; T. Holstein, *Ann. Phys.*, 1959, **8**, 343.
19 M. Cini, *J. Phys. C: Solid State Phys.*, 1986, **19**, 429.
20 M. Cini, *J. Phys. C: Solid State Phys.*, 1988, **21**, 193.
21 H. Sumi, *J. Phys. Soc. Jpn.*, 1974, **36**, 770; H. Sumi, *J. Phys. Soc. Jpn.*, 1975, **38**, 825.
22 N. Lu and S. Mukamel, *J. Chem. Phys.*, 1991, **95**, 1588.
23 J. Ye, Y. Zhao, N. Ng and J. S. Cao, *J. Phys. Chem. B*, 2009, **113**, 5897.
24 G. Whitfield and M. Engineer, *Phys. Rev. B: Solid State*, 1975, **12**, 5472.
25 K. Hannewald, V. M. Stojanović, J. M. Schellekens and P. A. Bobbert, *Phys. Rev. B*, 2004, **69**, 075221.
26 K. Huang and A. Rhys, *Proc. R. Soc. London, Ser. A*, 1950, **204**, 406.
27 J. Roden, A. Eisfeld, W. Wolff and W. T Strunz, *Phys. Rev. Lett.*, 2009, **103**, 058301.
28 V. L. Broude, E. I. Rashba and E. F. Sheka, *Spectroscopy of Molecular Excitons*, Springer, Berlin, 1985.
29 E. F. Sheka, *Sov. Phys. Usp.*, 1972, **14**, 484.
30 M. R. Philpott and J. M. Turlet, *J. Chem. Phys.*, 1976, **64**, 3852.
31 Q. M. Liu, Y. Zhao, W. H. Wang and T. Kato, *Phys. Rev. B: Condens. Matter Mater. Phys.*, 2009, **79**, 165105.
32 N. V. Prokof'ev and B. V. Svistunov, *Phys. Rev. Lett.*, 1998, **81**, 2514.
33 A. S. Mishchenko, N. V. Prokof'ev, A. Sakamoto and B. V. Svistunov, *Phys. Rev. B: Condens. Matter Mater. Phys.*, 2000, **62**, 6317.
34 J. Sun, B. Luo and Y. Zhao, to be published.